Proceedings of the 8th World Congress on Mechanical, Chemical, and Material Engineering (MCM'22)
Prague, Czech Republic – July 31, 2022 - August 02, 2022
Paper No. HTFF 131
DOI: 10.11159/htff22.131

Analytical Modelling on Simultaneous Phase Transitions in Low Temperature Evaporator for Organic Rankine Cycle Applications

Sandeep Aryal[1], Mohammad Abutayehb[2], Young Min Kim[3], Kwangkook Jeong[1]
[1]Arkansas State University, P.O. Box 1740, State University, AR, 72467, USA
sandeep.aryal@smail.astate.edu, kjeong@astate.edu
[2]Colorado State University, Fort Collins, CO 80523, USA
abutayeh@colostate.edu
[3]Korea Institute of Machinery and Materials, 171 Jang-dong, Yuseong-gu, Daejeon, 305-343, South Korea
ymkim@kimm.re.kr

Abstract

A lab-scale organic Rankine cycle has equipped a Low Temperature Evaporator (LTE) for water recovery in addition to the High Temperature Evaporator (HTE) for heat recovery. The recovered water is reused as the make-up water line to save the fresh water consumption in the cooling tower [1, 2]. Water recovery efficiency was defined as the ratio of the water condensation rate from the flue gas side to the moisture flowrate at the flue gas inlet [3]. The LTE as cross flow heat exchanger is to recover water in condensate form from the combustion flue gas in the duct side while the recovered latent and sensible heats are transferred into the refrigerant R134a in the tube side. The LTE involves complicated phenomena since the condensation of water vapour in the flue gas duct side and the flow boiling of R134a in tube side were taken place simultaneously. Design of a LTE and its optimized operation depend on a knowledge and understanding of the heat and mass transfer occurred in the LTE. Analytical modelling would be essential to derive the critical parameters for design and operation to achieve the goal of the organic Rankine cycle. The objective of this research was to develop an analytical modelling for simulating the simultaneous phase transitions: 1) condensation of water vapour in the duct side and 2) flow boiling of the refrigerant R134a in the tube side. The control volume was confined to the LTE with two working fluids including the combustion flue gas in the duct side and R134a in the tube side. The work scope was to conduct derivations of the governing equations and numerical algorithm, program development, validations and verifications, and extensive case studies. The modelling was able to generate the spatial profiles of temperature and heat transfer coefficients of both sides, vapour quality of R134a, and condensation rate of water vapour in flue gas side, etc. The mean absolute deviation between the calculated and measured heat transfer coefficients was within 18 %. The calculated data including exit temperature of flue gas and R134a, and water recovery efficiency were in good agreement with the measured data within 15 %. The case studies with the developed software were conducted to examine the roles of sensible and latent heat transfer in flue gas side and boiling impact of R134a side with variations of design and operating parameters including heat transfer area, and inlet conditions of flue gas and R134a, etc. The performance was compared with the case of water coolant under same conditions. The results show that the water recovery efficiency was able to enhance from the current 50 wt% to 77 wt% as expanding its total heat transfer area up to 4 times than the baseline dimension. It was found that the ratio of mass flow rate of the coolant to flue gas was a strong function to improve the water recovery efficiency due to the higher heat transfer coefficients in R134a side induced from the flow boiling. The comparison case study predicted the water recovery efficiency of the R134a case to be increased up to 20 wt%p than the water coolant case under same condition.

***Keywords*:** Analytical modelling, flow boiling of refrigerant, condensation of water, simultaneous phase change, heat and water recovery

1. Introduction

Thermoelectric power plants are one of the largest consumers of water in this world. According to United States Geological Survey (USGS), the total withdrawals for thermoelectric power in 2015 was 133,000 Mgal/day which was predominately freshwater [1]. The consumption of freshwater is so large that it is not sustainable for future and thus, new technologies have to be developed to reduce the amount of water use in the power industries. Exhaust gas from power plants contains large amount of water vapor and it has the potential to provide recovery of water and low-temperature heat. One of

the approaches is to recover water and heat from boiler flue gas by using condensing heat exchangers to absorb the low-temperature heat from flue gas into the coolant and to separate water vapor from flue gas in form of condensate.

This study aims to develop analytical modelling on heat and mass transfer in condensing heat exchanger by using refrigerant coolant (R134a) and study the feasibility of R134a in terms of water and heat recovery from low-temperature flue gas compared to typical water coolant to figure out the fundamental reasons that drive water and heat recovery performance and substitute coolant with enhanced water and heat recovery efficacy. An advanced organic cycle has been integrated with a high-temperature evaporator (HT-E) and low-temperature evaporator (LT-E) to respectively recover heat and water from the low-temperature combustion flue gas. In HT-E, the liquid refrigerant undergoes a phase transition to high-quality vapor to drive the turbine for generating additional power, while LT-E serves to recover water vapor as condensates from flue gas. In LT-E, the refrigerant R134a undergoes phase transition as well. Thus, in the heat exchanger, the condensation of water vapor occurs in flue gas side at the duct side and flow-boiling of the refrigerant in the tube side. This paper presents the modelling on pilot-scale LT-E to concentrate on simultaneous water condensation and flow-boiling of R134a and water recovery performance comparison between R134a and water coolant in LT-E.

In 1999, Yan et. al [2] investigated evaporative heat transfer and pressure drop for refrigerant R134a in a horizontal small circular pipe having an inside diameter of 2 mm and compared the heat transfer coefficient with pipes with a larger diameter. Kandlikar et. al [3] proposed a correlation of two-phase heat transfer coefficient for various refrigerants including R134a in mini-channel less than 3 mm for laminar and transition regions in 2004. This study was a modification to the previous work of Kandlikar [4,5] to propose the correlation for flow-boiling in minichannels. In 2005, Greco et. al [6] measured flow-boiling heat transfer coefficients of R134a at a horizontal tube with 6 mm internal diameter, mass velocity at 360 kg/sm^2, evaporating pressure at 3-12 bar, and heat flux at 11-21 kW/m^2. Saitoh et. al [7] developed a correlation to predict the heat transfer coefficient of R134a for horizontal tube and results showed that this correlation could be applied to a wide range of tube diameters ranging from 0.5-11 mm. In 2007, Choi et. al [8], studied convective boiling heat transfer in horizontal minichannels for different refrigerants including R134a and developed a boiling heat transfer coefficient correlation based on the superposition model.

Tibirica et. al [9] in 2009, presented an experimental flow-boiling heat transfer coefficient of R134a in a horizontal 2.32 mm internal diameter tube, mass velocity at 50-600 kg/sm^2, heat flux of 5-55 kW/m^2, and saturation temperature at 22 ºC, 31 ºC and 41 ºC. In 2010, Jeong et al. [10] developed analytical modelling to simulate heat and mass transfer in flue gas condensing heat exchangers to predict the water condensation rate from flue gas, and it showed good agreement with the measured data. In 2011, Copetti et. al [11] measured two-phase heat transfer coefficients of R134a in a horizontal mini tube with internal diameter 2.6 mm under the heat flux at 10-100 kW/m^2, mass velocity at 240-930 kg/sm^2, and saturation temperature 12-22 ºC. Jeong et. al [12] developed a numerical model to predict the simultaneous condensation and evaporation of water occurring in a high-pressure sorption unit to be used for IGCC (Integrated Coal Gasification Combined Cycle).

Kim and Mudawar [13] in 2013, proposed correlations to predict flow-boiling heat transfer of R134a in terms of two-phase heat transfer coefficient and dryout incipience under the hydraulic diameter of 0.19-6.5 mm, mass velocities 19-1,608 kg/sm^2, liquid only Reynolds number 57-49,820, qualities of 0-1, and reduced pressure of 0.005-0.69. Fang [14] proposed a correlation for flow-boiling based on the new dimensionless number Fa taking database consisting of 2,286 data points from various published papers. This new correlation also showed high prediction accuracy for other refrigerants. Similarly, Kim and Mudawar [15] in 2014, reviewed methods for predicting heat transfer in condensing and boiling mini/micro channels flows to access their accuracy. Sempértegui et. al [16] in 2016, investigated the effect of R134a on the heat transfer coefficient during flow-boiling inside the micro-scale channels, and this was the updated version of the predictive study by Kanizawa et. al [17].

Gorgy et. al [18] studied the experimental investigation on heat transfer performance and effect of tube pitch on the highly enhanced surface tube bundles with input variables: heat flux of 5-60kW/m^2, mass velocity 15-55 kg/sm^2, and quality of 0.1-0.7. This study proposed a new enhanced tube heat transfer coefficient bundle model. In 2019, Kim et. al [19] presented an experimental study on lab-scale ORC, and concluded that this ORC system could produce additional power from flue gas at 160 ºC with thermal efficiency of 3.3%, and aftercooler could recover 50% of water in the flue gas by cooling it below

30-40 ºC. In 2019, Shamsi et. al [20] studied a novel waste heat and water recovery system (WHWRS) integrated with ORC and cooling cycles using a singular working fluid undergoing a phase change. From this study, it was found that for a 600 MW power plant the water capture efficiency was 50%.

This paper describes numerical scheme on analytical modelling on simultaneous phase transitions (flow-boiling of R134a inside the tube and condensation of water vapors on the outer surface of tube) and compares water recovery performance from flue gas for R134a and water coolant. The modelling results are also compared with experimental data for the model verification and validation.

2. Theoretical

2.1. Control volume and main variables

The control volume used for the derivation of governing equations is shown in Fig. 1(a). A countercurrent cross-flow heat exchanger with smooth wall tubes is assumed. The flow of refrigerant R134a in the tube is horizontal. In Fig. 1(b), dependent variables and independent variables in the control volume which affect the water condensation are shown. $T_{fg,in}$ and $T_{fg,out}$ are flue gas inlet and outlet temperatures respectively in the control volume. R134a temperatures at the inlet and exit of the control volume are depicted as $T_{R134a,in}$ and $T_{R134a,out}$ respectively. The tube wall surface temperature is shown as T_w. The heat transfer in this control volume is governed by the heat transfer coefficient of flue gas side (h_{fg}) and R134a side (h_{R134a}).

The condensation of water vapor at the wall initiates where wall temperature is below the dew point temperature of water (T_{dew}) in flue gas side. $y_{H_2O,in}$ and $y_{H_2O,out}$ show the water vapor mole fraction at the inlet and exit respectively. The interfacial temperature of water between the flue gas and liquid film is denoted as T_i. The mass transfer coefficient of water vapor is denoted as k_m.

At coolant inlet side of the tube, R134a is initially in a subcooled state. Along the length of tube, as shown in Fig. 1, phase transition of R134a starts, and vapors of R134a start appearing by gaining heat from flue gas. R134a gains heat from both the sensible heat of flue gas and latent heat of condensation of water vapor. The latent heat gain to refrigerant is 0 in case of no condensation of water vapor. The vapor quality of R134a is represented as x. The heat transfer coefficient of R134a in two-phase flow is expressed as h_{tp}. In this study, both flue gas side and R134a side constitute the two phases. In case of water coolant in the heat exchanger, it remains subcooled liquid and does not undergo phase change.

2.2. Governing equations

Governing equations were derived to calculate the flue gas, refrigerant, and tube wall temperatures, water vapor mole fractions, and condensation rate of water vapor. The basic approach for the derivation of the governing equation is to use heat and mass transfer, and energy balances in the control volume. The various cases for the derivation of governing equations are shown.

2.2.1. Modelling for water vapor condensation in flue gas duct side

A. No condensation case in flue gas side and no phase transition of R134a inside the tubes

In a case of no condensation in the flue gas side and no phase change of R134a, the energy balance equations for both streams are given by:

$$\dot{m}_{fg} c_{fg} dT_{fg} = h_{fg}(T_{fg} - T_w) dA \quad (1)$$

$$\dot{m}_{R134a} c_{R134a} dT_{R134a} = h_{R134a}(T_w - T_{R134a}) dA \quad (2)$$

The flue gas and tube wall surface temperatures are calculated using Equations (1) and (2) respectively. In this case, the mass flow rate of wet flue gas remains constant due to no mass transfer.

B. Condensation in flue gas side and no phase transition of R134a inside the tubes

In the case of condensation in flue gas side, gas temperature can be found by modifying Equation (1), at which the wall temperature (T_w) is replaced with interfacial temperature (T_i), as the tube wall is assumed to be covered by liquid condensate film. The wall temperature can be still obtained from Equation (2). The interfacial temperature can be found by the Colburn-Hougen correlation [21] given by:

$$h_{fg}(T_{fg} - T_i) + k_m l_{lc}(y_{H_2O} - y_i) = U_o(T_i - T_{R134a}) \quad (3)$$

Subcooled R134a temperature due to sensible heat transfer can be found from Equation (4) given by:

$$[h_{fg}(T_{fg} - T_i) + k_m l_{lc}(y_{H_2O} - y_i)]dA = \dot{m}_{R134a} c_{R134a} dT_{R134a} \quad (4)$$

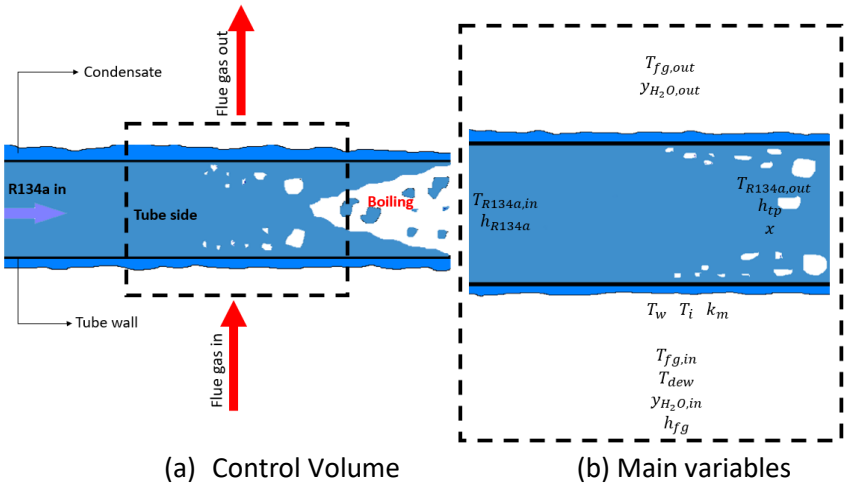

Fig. 1 Control volume (a) and main variables (b) for the analytical modelling

Water vapor condensation rate can be calculated using Equation (5) which is the function of mass transfer coefficient, mass gradient of water vapor between flue gas and interface, and contact area [10]. The condensation of water vapor causes change in mass flow rate of wet flue gas and it varies according to the amount of water vapor condensed from wet flue gas, while dry flue gas mass flow rate remains constant.

$$\dot{dm}_{cd} = k_m(y_{H_2O} - y_i)dA \quad (5)$$

The interfacial mole fraction of water vapor in Equation (5) is calculated using the Antoine equation [22]. This equation is a vapor-pressure equation in which the relation of saturated vapor-pressure and temperature of pure components are described. It is given by Equation (6) as:

$$y_i = \frac{exp\left(a - \frac{b}{T_i + c}\right)}{P_{tot}} \quad (6)$$

Here in Equation (6), a=16.262, b=3,799.89 and c=226.35. T_i and P_{tot} represent the temperature interfacial temperature in ºC and pressure in kPa.

C. Heat and mass transfer calculations in flue gas side

The thermal resistance of tube material is neglected in all the cases because the thickness of tube is thin and has high thermal conductivity. The Colburn j factors for heat and mass transfer with their ranges are given by [21,23]:

$$j_H = StPr^{\frac{2}{3}} = \frac{h_{fg}}{\rho c_p V} Pr^{\frac{2}{3}} \quad (7)$$

$$0.6 < Pr < 60$$

$$j_m = St_m Sc^{\frac{2}{3}} = \frac{k_m}{V} Sc^{\frac{2}{3}} \quad (8)$$

$$0.6 < Sc < 3{,}000$$

In Equation (7), h_{fg} is the convective heat transfer coefficient of flue gas side in W/m^{2}K, and in Equation (8), k_m is the convective mass transfer coefficient in m/s. The Chilton-Colburn analogy requires Equation (7) and (8), that is $j_H = j_m$.Then an expression for mass transfer coefficient, k_m, is derived as:

$$k_m = \frac{h_{fg} M_{H_2O}}{c_{p,fg} M_{fg} y_{lm} Le_{H_2O-gas}^{\frac{2}{3}}} \tag{9}$$

The logarithmic mole fraction of non-condensable gas across the film in Equation (9) is given by [24,25]:

$$y_{lm} = \frac{y_{ni} - y_{nb}}{ln\left(\frac{y_{ni}}{y_{nb}}\right)} \tag{10}$$

In Equation (10), y_{ni} and y_{nb} represents the mole fractions of non-condensable gases at the interface and in bulk flue gas flow, respectively. The Lewis number of water vapor in flue gas is given by:

$$Le_{H_2O-gas} = \frac{Sc}{Pr} = \frac{\alpha_g}{D_{H_2O-gas}} \tag{11}$$

In Equation (11), D_{H_2O-gas} represents the binary mass diffusion coefficient of water vapor in flue gas.

The convective heat transfer coefficient on flue gas side of a bare tube bank is predicted using the empirical correlation proposed by Zukauskas [26], given by:

$$Nu_{fg} = C_1 Re_{fg}^m Pr_{fg}^{0.36} \left(\frac{Pr_{fg}}{Pr_s}\right)^{0.25} \tag{12}$$

Equation (12) is valid if $N_l \geq 20$ and for $N_l < 20$,Equation (12) is modified as:

$$Nu_{fg} = C_1 C_2 Re_{fg}^m Pr_{fg}^{0.36} \left(\frac{Pr_{fg}}{Pr_s}\right)^{0.25} \tag{13}$$

For $Re_{fg} \leq 100$, $C_1 = 0.8$ and $m = 0.4$, $Re_{fg} \leq 1000$, $C_1 = 0.51$ and $m = 0.5$, $Re_{fg} \leq 200{,}000$, $C_1 = 0.27$ and $m = 0.63$, and $Re_{fg} \leq 2{,}000{,}000$, $C_1 = 0.021$ and $m = 0.84$. The constant C_2 is calculated using interpolation from N_l and C_2 values.

Water vapor condensation rate is defined as the total amount of water vapor condensed on outer tube surface from incoming wet flue gas. This condensation rate allows to calculate water recovery efficiency. The water recovery efficiency on weight basis is defined as the ratio of total water vapor condensation rate in kg/s to the mass flow rate of water vapor in incoming wet flue gas in kg/s and is calculated using Equation (14) as:

$$\eta_{cd}[wt.\%] = \frac{\dot{m}_{cd}}{\dot{m}_{H_2O,in}} \times 100 \tag{14}$$

2.2.2 Modelling for refrigerant flow-boiling in coolant tube side

A. No boiling of R134a inside tubes

The single-phase flow heat transfer coefficient of R134a inside the tube is calculated using Gnielinski's correlation which is valid for either pure liquid or pure vapor as given by Equation (15):

$$Nu_D = \frac{\frac{f}{8}(Re_{R134a} - 1000)Pr}{1 + 12.7\left(\frac{f}{8}\right)^{0.5}\left(Pr^{\frac{2}{3}} - 1\right)} \tag{15}$$

This equation is valid only for $0.5 \leq Pr \leq 2{,}000$ and $3{,}000 \leq Re_{R134a} \leq 5{,}000{,}000$. In the case of laminar flow with constant surface temperature, both the friction factor and the heat transfer coefficient remain constant in the fully developed region and Nusselt number is given by [27]:

$$Nu_D = \frac{h_{R134a} D}{\lambda_{R134a}} = 3.66 \tag{16}$$

For the fully developed flow with constant heat flux, Nusselt number is independent of Reynolds and Prandtl numbers and is given by [27]:

$$Nu_D = \frac{h_{R134a} D}{\lambda_{R134a}} = 4.36 \tag{17}$$

B. Flow-boiling of R134a inside tubes

The initiation of vapor formation in subcooled liquid starts when the tube wall temperature remains essentially constant, a few degrees above the saturation temperature. Since the flow is circulated by pump, the fluid and thermal transport regimes are governed by forced convective flow-boiling. The boiling heat transfer coefficients of R134a were calculated by using the correlation developed by Kim and Mudawar [13] under the following constraints:

- Working fluid: FC72, R11, R113, R123, R1234yf, R1234ze, R134a, R152a, R22, R236fa, R245fa, R32, R404A, R407C, R410A, CO_2 and water
- Hydraulic diameter: $0.19 \leq D_h \leq 6.5$ mm
- Mass velocity: $19 < G < 1{,}608$ kg/m^{2}s
- Liquid-only Reynolds number: $57 < Re_{fo} < 49{,}820$
- Vapor quality: $0 < x < 1$, and
- Reduced pressure: $0.005 < P_R < 0.69$

The boiling heat transfer coefficient for the nucleate boiling regime and the convection boiling regime were calculated using Equations (18) and (19) respectively:

$$h_{nb} = \left[2345\left(B_o \frac{P_H}{P_F}\right)^{0.7} P_R^{0.38}(1-x)^{-0.51}\right]\left(0.023 Re_f^{0.8} Pr_f^{0.4} \frac{\lambda_f}{D_h}\right) \tag{18}$$

$$h_{cb} = \left[5.2\left(B_o \frac{P_H}{P_F}\right)^{0.08} We_{fo}^{-0.54} + 3.5\left(\frac{1}{X_{tt}}\right)^{0.94}\left(\frac{\rho_g}{\rho_l}\right)^{0.25}\right]\left(0.023 Re_f^{0.8} Pr_f^{0.4} \frac{\lambda_f}{D_h}\right) \tag{19}$$

The associated variables in Equations (18) and (19) are given as:

$$\text{Boiling number: } B_o = \frac{q_H^{"}}{G l_{R134a}} \tag{20}$$

Boiling number (B_o) is a dimensionless number which gives the ratio of actual heat flux ($q_H^{"}$) to the maximum attainable heat flux ($G \times l_{R134a}$) from complete evaporation of liquid. In Equation (20), G and l_{R134a} are the mass velocity and latent heat of R134a respectively flowing inside the tube respectively.

$$\text{Reduced pressure: } P_R = \frac{P}{P_{crit}} \tag{21}$$

$$\text{Superficial liquid Reynolds number: } Re_f = \frac{G(1-x)}{\mu_f} \tag{22}$$

$$\text{Weber number: } We_{fo} = \frac{G^2 D_h}{\rho_f \sigma} \tag{23}$$

X_{tt} is the Lockhart-Martinelli parameter based on the liquid-turbulent vapor flows and is calculated using Equation (24):

$$X_{tt} = \left(\frac{\mu_f}{\mu_g}\right)^{0.1}\left(\frac{1-x}{x}\right)^{0.9}\left(\frac{\rho_g}{\rho_f}\right)^{0.5} \tag{24}$$

Lockhart-Martinelli is a dimensionless parameter used to express liquid fraction in multi-phase flows.

The two-phase heat transfer coefficient, h_{tp} is the function of the nucleate boiling heat transfer coefficient and convective heat transfer coefficient as given by Equation (25):

$$h_{tp} = \left(h_{nb}^2 + h_{cb}^2\right)^{0.5} \tag{25}$$

In the case of the dryout, dryout incipience quality for the saturated flow-boiling is predicted using Equation suggested by Kim and Mudawar, given as:

$$x_{di} = 1.4 We_{fo}^{0.03} P_R^{0.08} - 15.0\left(B_o \frac{P_H}{P_F}\right)^{0.15} Ca^{0.35}\left(\frac{\rho_g}{\rho_l}\right)^{0.06} \tag{26}$$

In Equation (26), Ca is the Capillary number calculated as :

$$Ca = \frac{\mu_f G}{\rho_f \sigma} = \frac{We_{fo}}{Re_{fo}} \tag{27}$$

At the dryout incipience point, two phase heat transfer significantly decreases and the wall temperature rises sharply.

The governing equations used in water coolant for heat and mass transfer modelling in this paper are described in the paper by Jeong et al. [10].

3. Numerical methods

For the numerical modelling, a pilot-scale LT-E was considered as a cross-flow heat exchanger with internal diameter of 6.5 mm and total outer surface area equal to 1.54 m^2. The total number of tubes in this heat exchanger were 225. The detailed geometric dimensions of LT-E are listed in Table 1.

Table 1. Geometrical dimensions of Low Temperature Evaporator

Type	Pilot-scale horizontal cross-flow heat exchanger
Outer diameter	7.3 mm
Internal diameter	6.5 mm
Transverse pitch	26 mm
Longitudinal pitch	78 mm
Tube bank	9 rows X 25 columns
Total number of tubes	225
Duct dimension	0.3 m X 0.233 m X 1.94 m

The cross-flow heat exchanger was discretized into 15,400 cells with each cell having an area of 0.0001 m^2 to produce enhanced computation results between calculation time and accuracy. The governing equations corresponding to the boundary value problem were solved by using an iterative solution technique and single tube method with the 1-D forward finite difference method (FDM) [28,29]. The inlet conditions of both flue gas and refrigerant R134a sides were assumed to be known with temperature, mass flow rate, and chemical composition of the flue gas. The phase of refrigerant at inlet of the tube is set at subcooled liquid at the given pressure.

There were three possibilities for refrigerant at the exit conditions: subcooled liquid (l), saturated liquid-vapor mixture (l+v), and superheated vapor (v) as shown in Fig. 2. Flue gas exit temperature and the state of refrigerant were obtained using iteration by assuming an exit condition for refrigerant and integrating backward to match the inlet condition of refrigerant at the entrance of tube side. Three loops were employed to iterate on those possible exit states of the refrigerant.

First loop (ITER-1) assumes no phase transition ($x = 0$) at the refrigerant side and iterates on the exit refrigerant temperature until the calculated inlet and refrigerant temperature approaches the target inlet temperature in tube side. ITER-1 calculates the condensation rate on flue gas side without evaporation of refrigerant inside the tube. During the loop, inner and outer tube wall temperature stays below the saturation temperature of refrigerant everywhere in the heat exchanger. The only assumed variable is the coolant exit temperature.

If refrigerant is assumed to leave the tube at exit as a liquid-vapor mixture and ITER-1 does not meet the boundary conditions, the loop (ITER-2) is executed. The modelling program calculates the phase changes for cases: a) the internal tube wall temperature is higher than the saturation temperature of refrigerant to evaporate the refrigerant, and b) the outer tube wall temperature is lower than the saturation temperature of water moisture in the flue gas to condense. So it allows simultaneous phase transitions inside the tube (flow-boiling of refrigerant) and outer surface of tube (condensation from flue gas side). The algorithm iterates with the assumed quality of refrigerant for the range of $0 < x < 1$ until the calculated refrigerant temperature reaches the target inlet temperature of refrigerant in the tube side. In this loop, the only assumed variable is refrigerant quality at the exit since the refrigerant temperature is assumed to be at saturation temperature.

If refrigerant leaves the heat exchanger at superheated vapor ($x = 1$) and none of ITER-1 and ITER-2 converges, the third loop (ITER-3) begins with an assumption of exit superheated refrigerant temperature. ITER-3 computes phase transition from the subcooled liquid to superheated vapor in the refrigerant side with the possibility of condensation of water vapor in flue gas side. The algorithm iterates with the assumed temperature of exit superheated refrigerant until the calculated refrigerant temperature reaches the given target inlet temperature in tube side. For all the loops convergence criteria (

$\left|\frac{T_{ref,in,calc}-T_{ref,in,target}}{T_{ref,in,target}}\right|$) for the calculated and target inlet temperature of the refrigerant was set at 0.001 using the sensitivity analysis because the convergence criteria less than 0.001 had no significant effect on outcome of modelling results.

The current model yields the distribution profiles of temperatures, mole fractions, local condensation rates of water vapor in the flue gas side, vapor qualities of refrigerant sides to predict the heat transfer rates, mass transfer rates, and the water recovery efficiency. The database of all the properties was built using the NIST (National Institute of Standards and Technology) [30]. The program was coded and executed in MATLAB R2020a. For water coolant, a similar modelling strategy was applied. The only difference in water coolant case was that the quality and superheated vapor stage of water at the exit need not to be assumed because the water at the exit is subcooled liquid.

4. Experimental

To study the flow-boiling of refrigerant R134a and water recovery efficiency on flue gas side, an evaporator with the similar modelling specifications was placed by the Korea Institute of Machinery and Materials (KIMM) for experimental purpose. The liquid refrigerant R134a was routed to the inlet of tube and was heated by flue gas exhausted from the combustion of natural gas. The test section was a shell and tube heat exchanger and had an area of 1.54 m^2. The inner and outer diameters of tube were 6.5 mm and 7.3 mm respectively. Flowmeter was installed at the inlet of tube in the evaporator to measure R134a flow rate. A humidity meter was installed at the inlet and exit of the heat exchanger to measure the relative humidity of flue gas. The temperatures were also measured at the inlet and outlet of both R134a and flue gas sides.

The mole fraction of water vapor present at the inlet and exit of the heat exchanger was calculated using the relation between relative humidity and saturation pressure of water vapor. The mole fraction is calculated by Equation (28):

$$y_{H_2O} = \frac{\phi P_{sat,H_2O}}{P_{tot}} \tag{28}$$

The calculated mole fraction of water vapor present in flue gas is converted into a mass flow rate by Equation (29):

$$\dot{m}_{H_2O} = \frac{y_{H_2O} M_{H_2O} \dot{m}_{fg}}{M_{fg}} \tag{29}$$

The difference between the inlet and outlet mass flow rate of water vapor is defined as the condensation rate of the water vapor in the flue gas. Thus, the measured water condensation efficiency is calculated using Equation (14).

The heat transfer rate from flue gas is measured from the enthalpy change of flue gas, and the heat gained by R134a is measured from enthalpy change of R134a. Equations (30) and (31) are employed to measure the heat transfer rates, as given by:

$$\dot{Q} = \dot{m}_{fg,in} e_{fg,in} - \dot{m}_{fg,out} e_{fg,out} \tag{30}$$

$$\dot{Q} = \dot{m}_{R134a,in} e_{R134a,in} - \dot{m}_{R134a,out} e_{R134a,out} \tag{31}$$

5. Results and Discussions

The calculated boiling heat transfer coefficients were validated by comparing with measured data as shown in Fig. 3. The calculated boiling heat transfer coefficients were validated quantitatively and qualitatively with measured data under mass velocity $G = 371$ kg/sm^2 from Greco et al. [6] in Fig. 3. The correlations from Fang et al. [14] were also applied to the modelling to check heat transfer coefficient of R134a. It was observed that heat transfer coefficients calculated from Fang's correlations was 29% higher than predicted by Kim and Mudawar's correlations. From Fig. 3, it was seen that modelling results from Fang follow the measurements from Greco at $P = 4.1$ bar and $q^{"} = 15.8$ kW/m^2, while Kim and Mudawar follow measurements at $P = 3.3$ bar and $q^{"} = 10.9$ kW/m^2, however, in both the correlations, P was 7.94 bar and $q^{"}$ was 8.8 kW/m^2. In this modelling, correlations from Kim and Mudawar was used because heat transfer coefficient results showed close proximity with Greco's measurements, however, $q^{"}$ in modelling showed deviation from Greco's by 19.2%. It is preferable to use Fang's correlation for $D_h < 3$ mm than $D_h \geq 3$ mm because it has much better prediction performance in $D_h < 3$ mm. From Fang's prediction analysis, Mean Absolute Deviation (MAD) of heat transfer coefficients for $D_h < 3$ mm is 13.1%, however, MAD for $D_h \geq 3$ mm is 18.1% [14].

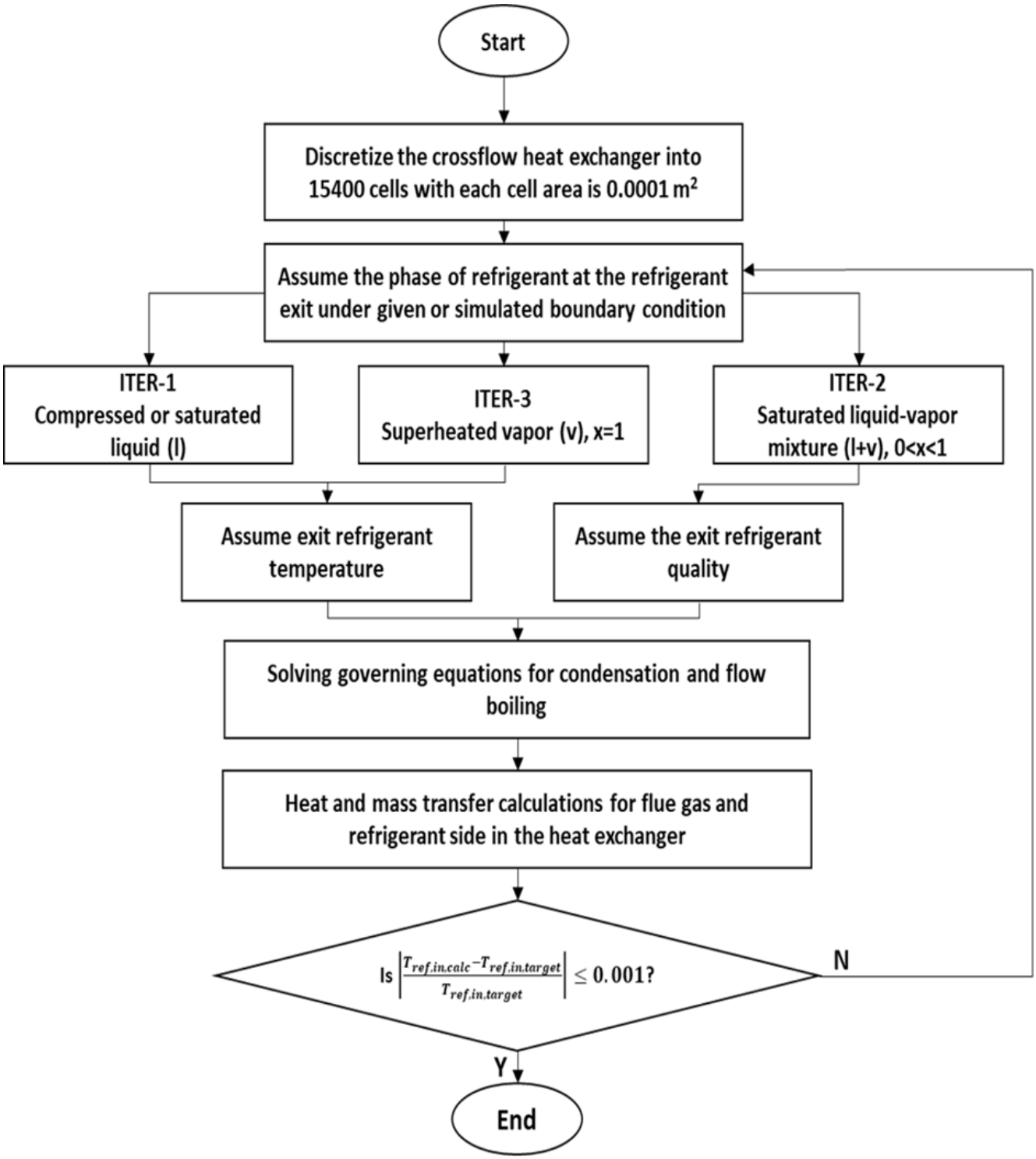

Fig. 2. Numerical algorithm of the analytical modelling

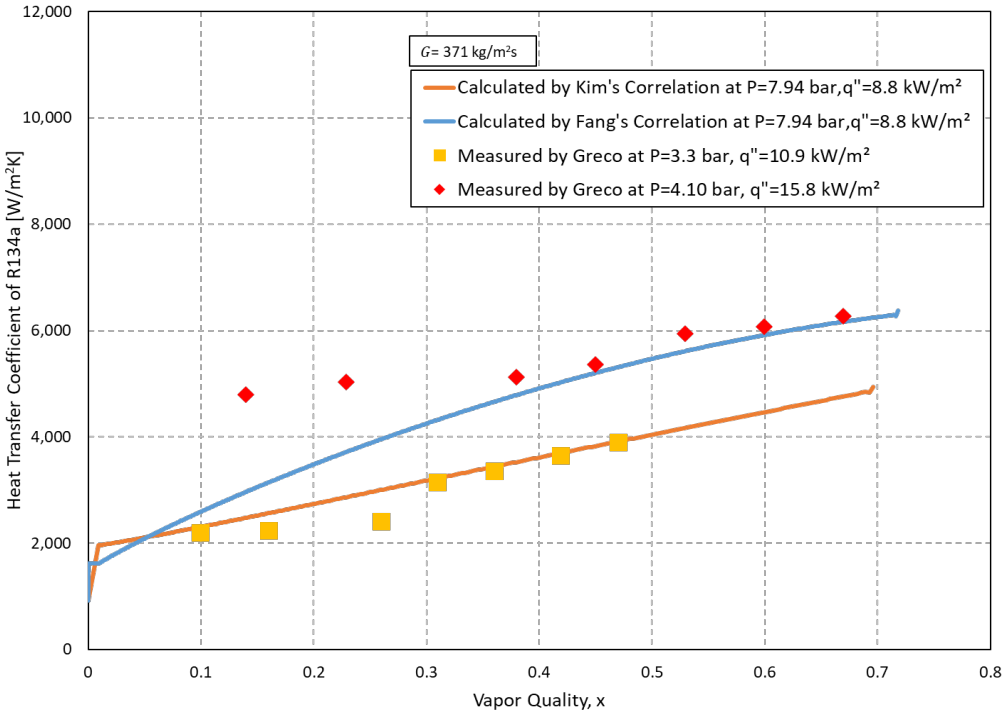

Fig. 3 Heat transfer coefficients comparison of R134a with different correlations and measured data

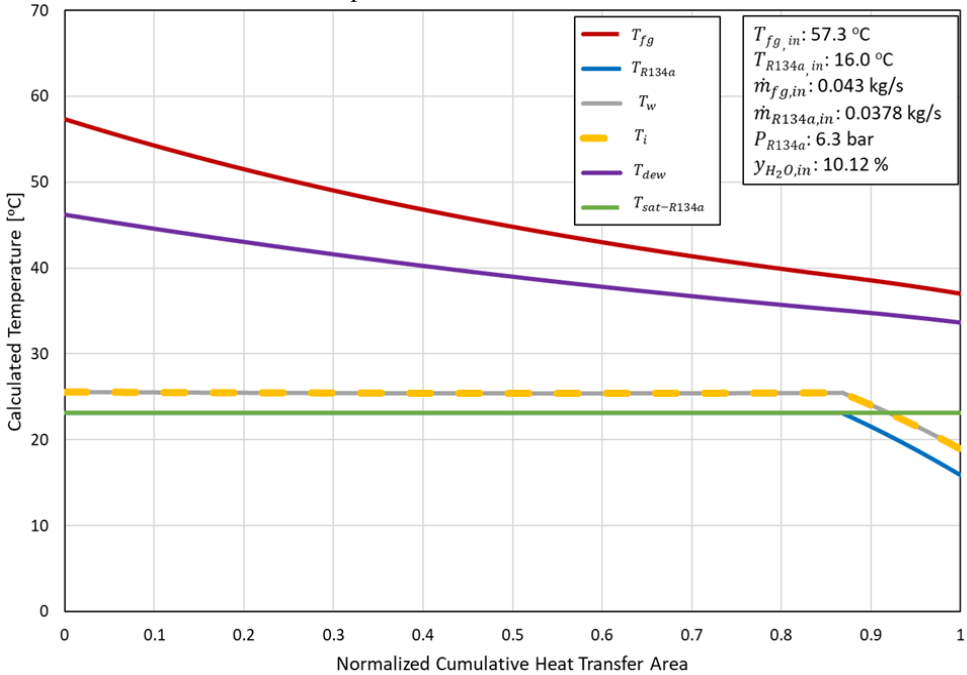

Fig. 4 Calculated temperature profiles along the normalized cumulative heat transfer area for R134a coolant

As shown in Fig. 4, modelling was conducted to calculate the temperature profiles of a total of six variables including flue gas, tube wall surface, interfacial, R134a saturation, and water vapor dew point in LT-E. The wet flue gas inlet temperature and mass flow rate were 57.3 °C and 0.043 kg/s respectively. R134a temperature, mass flow rate and pressure

at the inlet were 16.0 ºC, 0.038 kg/s, and 6.3 bar respectively. These boundary conditions were taken from the pilot-scale test setup used for experimental purpose.

The calculated flue gas exit temperature from the modelling was 37 ºC and R134a exit temperature was 23.1 ºC. The calculated tube wall surface and interfacial temperatures remained closed to each other as shown in Fig. 4, but interfacial temperature slightly exceeded the wall temperature by 0.06 ºC on average basis. On R134a side, where the tube wall surface temperature was lower than saturation temperature of R134a, there was only sensible heat transfer (no phase change) and it was marked by the increase in the temperature of R134a. When the tube wall surface temperature was higher than saturation temperature of R134a, there was only latent energy change in R134a side due to flow-boiling. This was marked by the constant temperature of R134a in LT-E and this constant temperature (23.1 ºC) was reached when the area of LT-E was 0.18 m^2 from inlet of R134a side as shown in Fig. 4. However, in flue gas side, there was both sensible and latent heat transfer. Since, interfacial temperature was always lower than dew point temperature of water in flue gas, there was condensation of water vapor from flue gas from inlet to exit of L-TE which contributed to latent heat transfer.

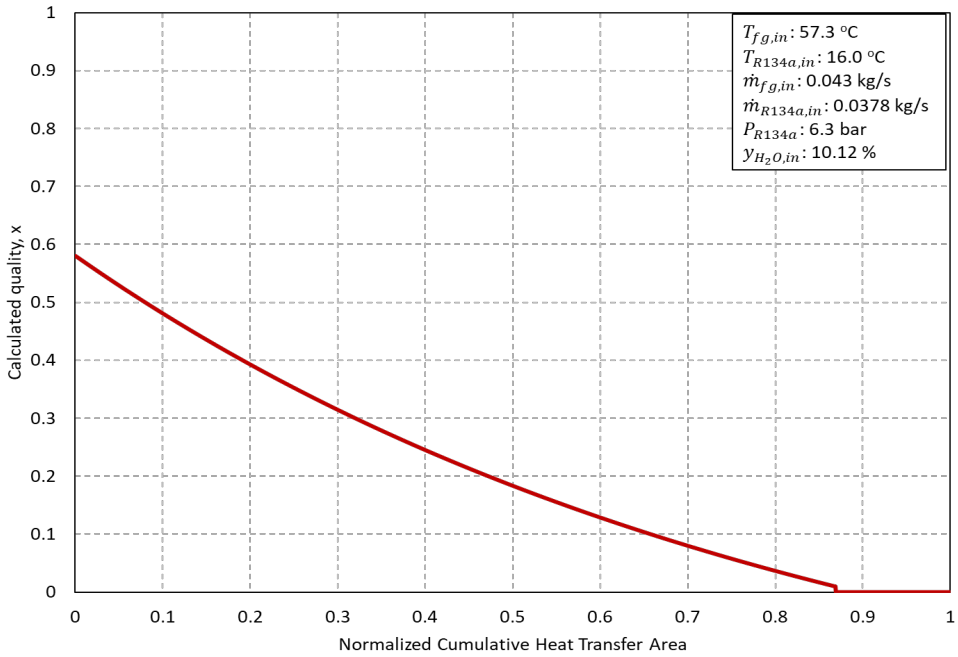

Fig.5 Calculated profile of vapor quality of R134a along the normalized cumulative heat transfer area

The calculated vapor quality of R134a from inlet to exit was depicted in Fig. 5. At the inlet of LT-E, R134a was subcooled liquid. As R134a further flowed along the heat exchanger, by absorbing heat from flue gas through the tube wall, it started to evaporate. The evaporation of R134a led to the formation of its vapor. At the inlet of R134a, the vapor quality is initially 0, and as it gained heat from flue gas, its temperature increased to its saturation temperature. At the region where the temperature of tube wall surface is higher than saturation temperature of R134a, the vapor of R134a started to appear when $x > 0$ as shown in Fig. 5. The calculated vapor quality of R134a at the exit of LT-E was 0.58. The temperature of R134a remained at saturation temperature from the start of vapor formation until the exit of LT-E because of only latent heat transfer in R134a. For this case, there was no dryout in LT-E because gradual thinning of liquid film traveling along the tube was not sufficient enough, 42% of R134a still existed as liquid in saturated-liquid vapor mixture and the predicted dryout incipient quality from the modelling was 0.85 by using Equation (26) but this did not happen in LT-E.

For the validation of modelling results from R134a coolant, the experimental boundary conditions were entered in the modelling. The mass flow rate of flue gas, flue gas inlet temperature, and mole fraction of water vapor in flue gas at the inlet were varied from 1.9-2.03 kg/min, 50.02-57.26 ºC, and 9.64-11.51% respectively both in the test and modelling. Fig. 6

showed the comparison between measured and calculated water condensation efficiency. The dotted line in Fig. 6 showed the ±15% standard deviation band. All the calculated data were within ±15% with an average discrepancy of 10% between measured and calculated data.

Under the same boundary conditions, flue gas exit temperatures were also compared with measured and calculated data as shown in Fig. 7. The dotted line in Fig. 7 also showed the ±15% standard deviation band. All the calculated data were within ±15 % with an average discrepancy of 3% with measured data. The discrepancy between the two sets of data in both Fig. 6 and 7 may be resulted from measurement uncertainty, accuracy of the correlations and numerical modelling method itself. Therefore, it can be concluded that this modelling method was able to calculate heat and mass transfer in LT-E with good accuracy.

Heat transfer coefficients of flue gas and coolant for both R134a and water coolant case were shown in Fig. 8 for performance comparison. The boundary conditions for R134a and water coolant was kept same except the inlet pressures for R134a and water coolant were 6.3 and 1 bar respectively. For R134a, the heat transfer coefficient of flue gas was 30.5-28 W/m2K, while for water coolant case heat transfer coefficient of flue gas was 30.2-29 W/m2K. The heat transfer coefficient of flue gas in both cases did not differ much because there was essentially no variation in the velocity of flue gas which in turn did not impact Reynolds number of flue gas (average $Re_{fg} = 362$ for R134 and $Re_{fg} = 343$ for water) and, Reynolds did not impact Nusselt number of flue gas. Thus, with no significant change in Nusselt number of flue gas in both coolant cases, the heat transfer coefficient of flue gas showed no significant deviations.

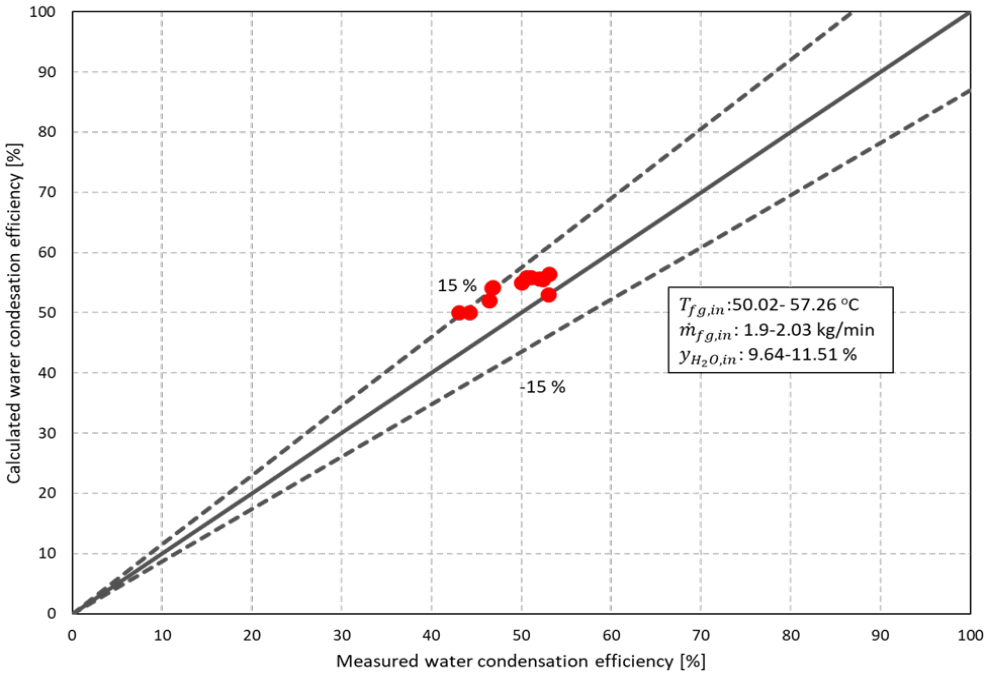

Fig. 6. Comparison between calculated and measured water recovery efficiency

For subcooled region of R134a, its heat transfer coefficient was 708 W/m^{2}K, however, with occurrence of phase transition, heat transfer coefficient of R134a in two-phase was accompanied with rise in its value reaching 1,897 W/m^{2}K at its exit. The reason for increase in two-phase heat transfer coefficient (h_{tp}) of R134a is due to increase in the void fraction (portion of flow passage volume occupied by R134a vapors) which decreases the density of liquid-vapor mixture and consequently increases the flow velocity of R134a. This increase in flow velocity increases Reynolds number (average $Re_f = 3230$), which ultimately increases the two-phase heat transfer coefficient.

For water coolant case, the heat transfer coefficient of water ranged from 405 to 423 W/m^{2}K from its inlet to exit. The water heat transfer coefficient did not rise as higher as R134a because no phase transition occurred in the tube side. The total heat transfer rate in LT-E with R134a coolant was in 6 kW while for water coolant it was 4 kW, and this higher heat transfer rate with R134a coolant was resulted from the higher two-phase heat transfer coefficient. From the performance comparison between two coolant cases, it was found that heat exchange between flue gas to coolant was 50% more effective in R134a than in water coolant.

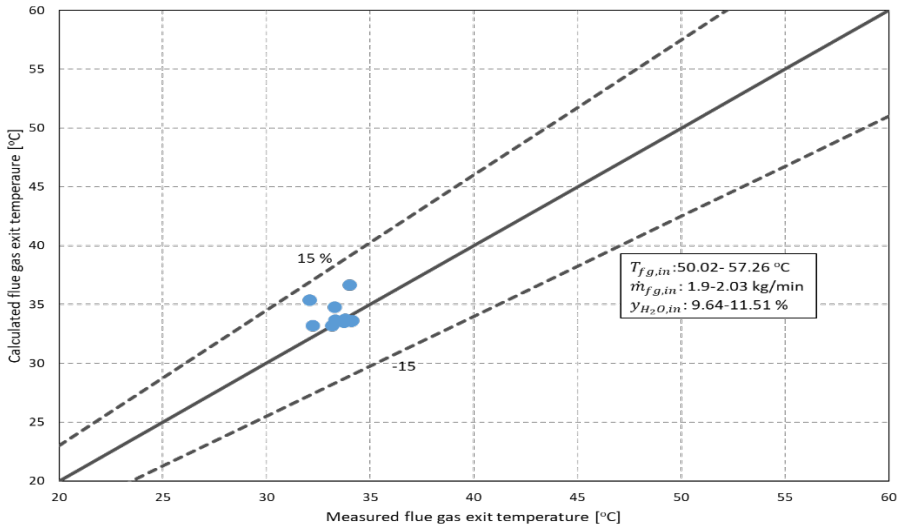

Fig. 7. Comparison between calculated and measured flue gas exit temperatures

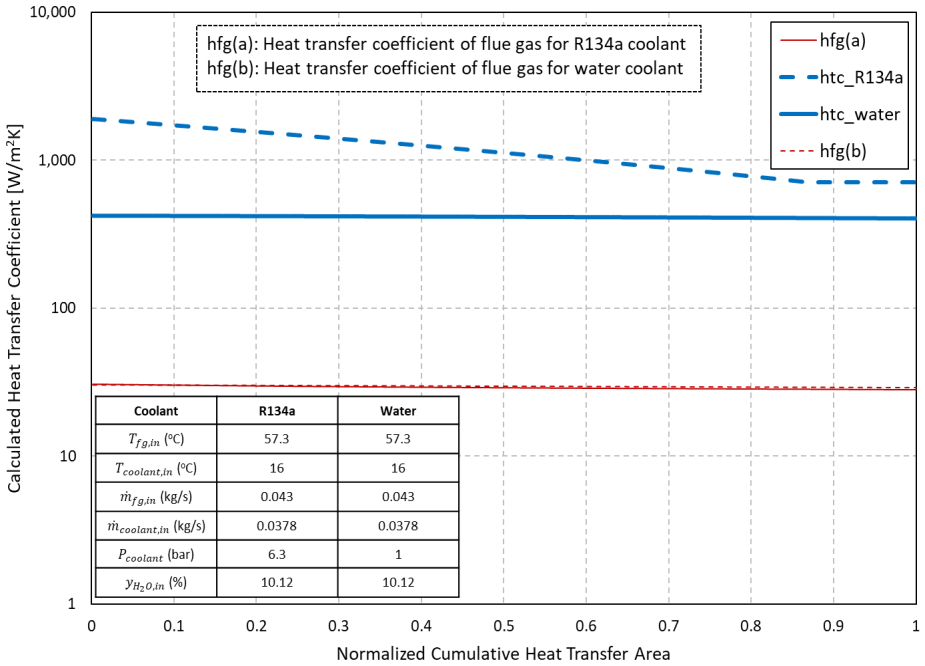

Fig. 8. Calculated heat transfer coefficients of flue gas and coolants along the normalized cumulative heat transfer area for two cases: a. R134a as coolant and, b. Water as coolant

Fig. 9 showed temperature profiles of flue gas, water, tube wall surface, interfacial and water vapor dew point for water coolant routed in the heat exchanger. The simulations were performed with same boundary conditions as in R134a coolant

except pressure which was 1 bar in water in order to compare the performance of both coolants. The modelling results showed that temperature of flue gas decreased from 57.3 ºC to 42 ºC from inlet to exit of flue gas side while water temperature increased from 16 ºC to 39 ºC from inlet to exit. As shown in Fig. 9, interfacial temperature was always less than dew point temperature of water in flue gas and hence condensation of water vapor occurred throughout the heat exchanger from inlet to exit. The comparison between temperature profiles of R134a and water coolant showed that R134a was able to cool down flue gas to a lower temperature than water due to enhanced heat transfer coefficient of R134a resulted from flow-boiling.

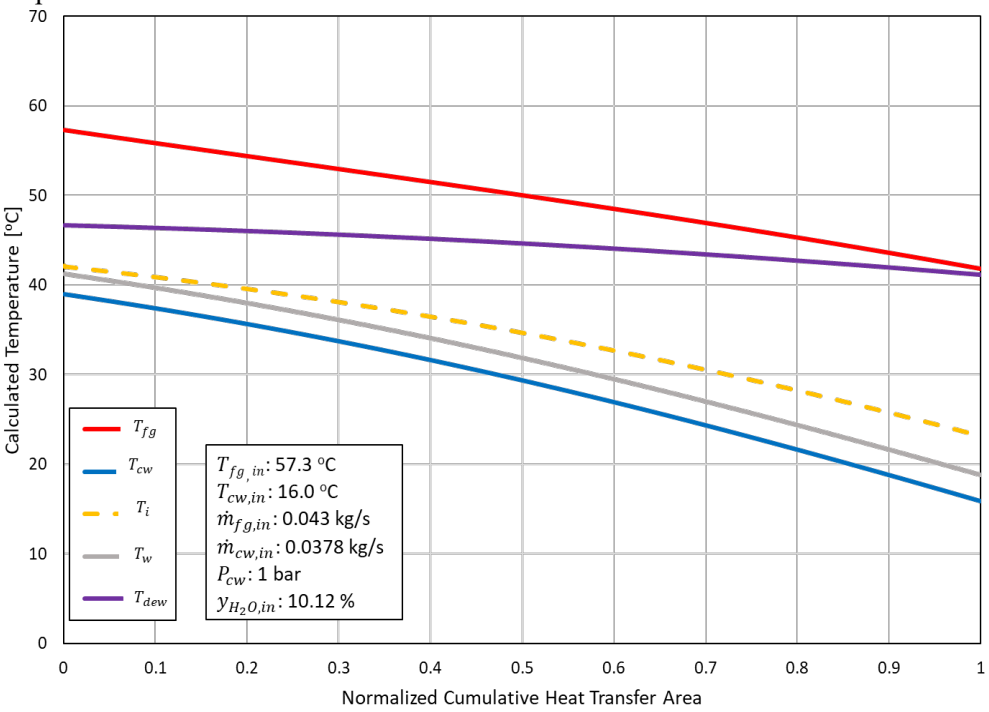

Fig. 9. Calculated temperature profiles along the normalized cumulative heat transfer area for water as coolant

Fig. 10 (a) and (b) represented the calculated mole fraction of water vapor at bulk and interface for R134a and water coolant respectively along the normalized cumulative heat transfer area in order to investigate and compare the water recovery performance. The calculated mole fraction of water vapor at bulk decreased from 0.1012 to 0.05 for R134a, and for water coolant, it decreased from 0.1012 to 0.075 because of condensation of water vapor on tube surfaces.

From Fig. 10 (a) for R134a, it was observed that interfacial mole fraction of water vapor remained constant to 0.032 until the point where the cumulative area of LT-E was 1.36 m2 from inlet of flue gas side because interfacial mole fraction of water vapor remains constant when interfacial temperature is constant as shown in Fig. 4, assuming negligible pressure drop of flue gas as explained by Antoine Equation (6). Then the interfacial mole fraction of water vapor started to decline and reached to 0.021 because interfacial temperature decreased from the point when cumulative area was 1.36 m^2 until the exit of LT-E in flue gas side. However, for water coolant in Fig. 10 (b), interfacial mole fraction of water vapor decreased monotonously from 0.08 to 0.027 along the heat exchanger area. For water coolant case in Fig. 10 (b), the interfacial mole fraction did not follow the same trend as in R134a because interfacial temperature was varying along the heat exchanger from inlet to exit as shown in Fig. 9.

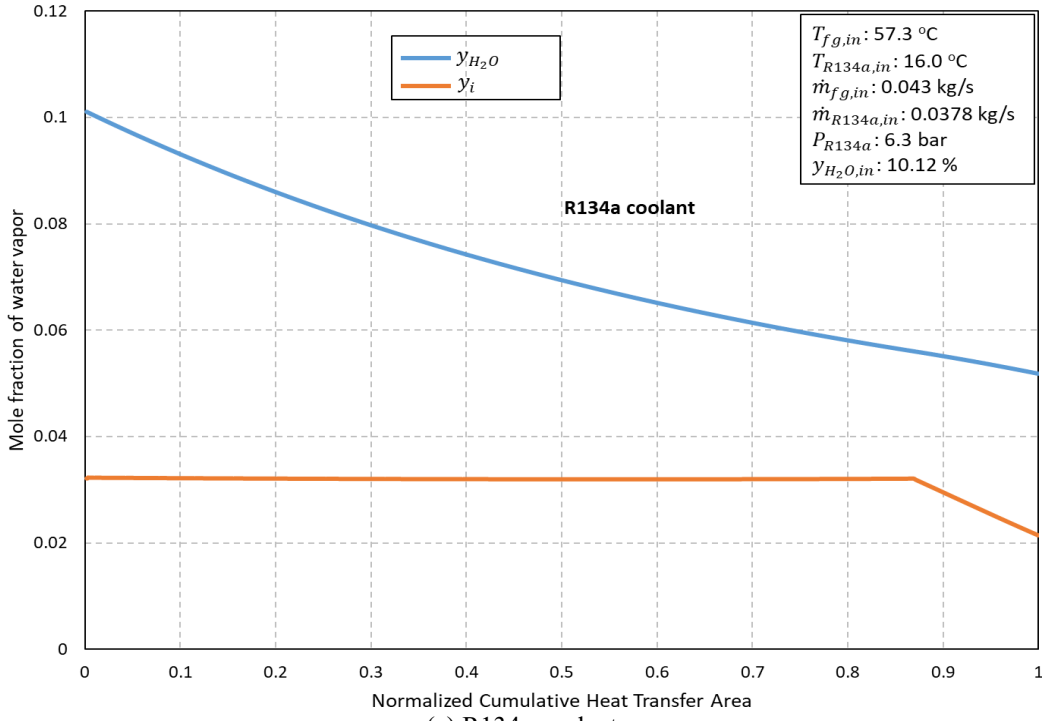

(a) R134a coolant case

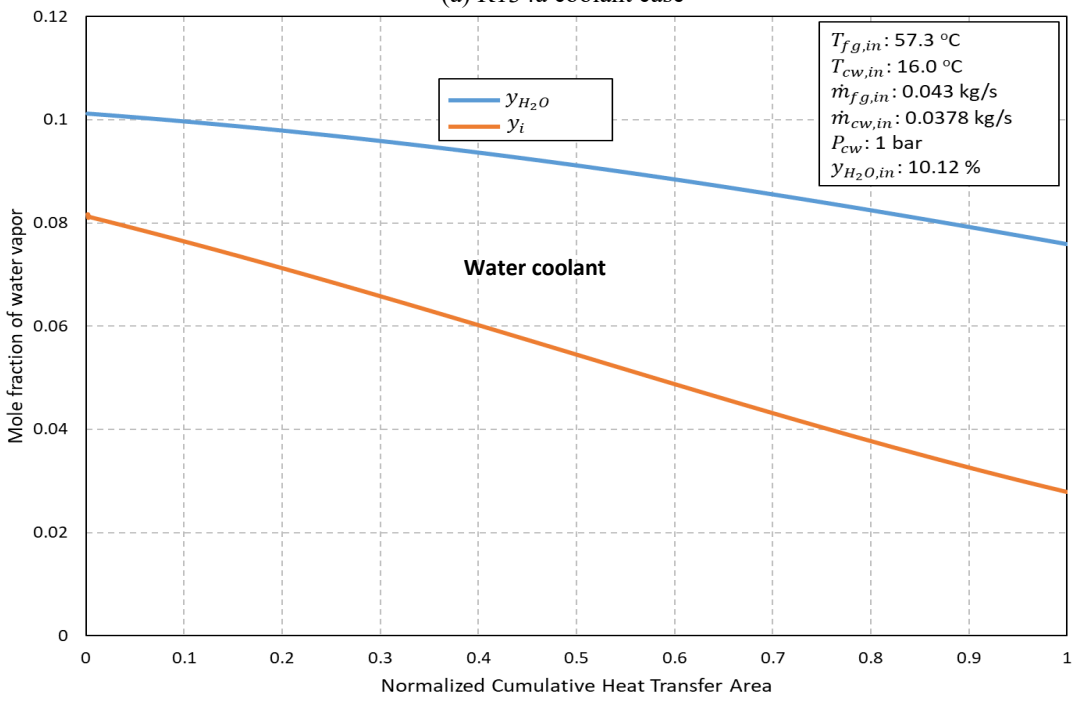

(b) Water coolant case

Fig. 10. Calculated bulk and interfacial mole fraction of water vapor along the normalized cumulative heat transfer area for (a) R134a coolant and (b) Water coolant case

Comparison between calculated water recovery rate from flue gas side along the normalized cumulative heat exchanger area for R134a and water coolant was shown in Fig. 11. The condensation of water vapor starts when the tube wall surface

temperature gets lower than dew point temperature of water vapor in flue gas. As depicted in Fig. 4 and 9, it was evident that this condition was met. For R134a case, as seen in Fig. 11, the local condensation rate decreased from 1.48 mg/s to 0.51 mg/s until the point when the cumulative heat exchanger area was 1.36 m^2 and after that point condensation rate increased to 0.64 mg/s. The condensation rate was highest at inlet side of flue gas because molar gradient of water vapor between bulk and interface $(y_{H_2O} - y_i)$ was greatest at inlet of flue gas side, and along the heat exchanger area it monotonously decreased until the point where area is 1.36 m^2 as inferred from Fig. 10 (a). The condensation rate then showed an increasing trend after this point in L-TE because of an increase in $(y_{H_2O} - y_i)$ as shown in Fig. 10 (a). The total condensation rate was calculated by integrating the local condensation rate along LT-E in the modelling. The total condensation rate calculated was 1,340 mg/s. Water recovery efficiency (wt. basis) predicted from this modelling was 50%.

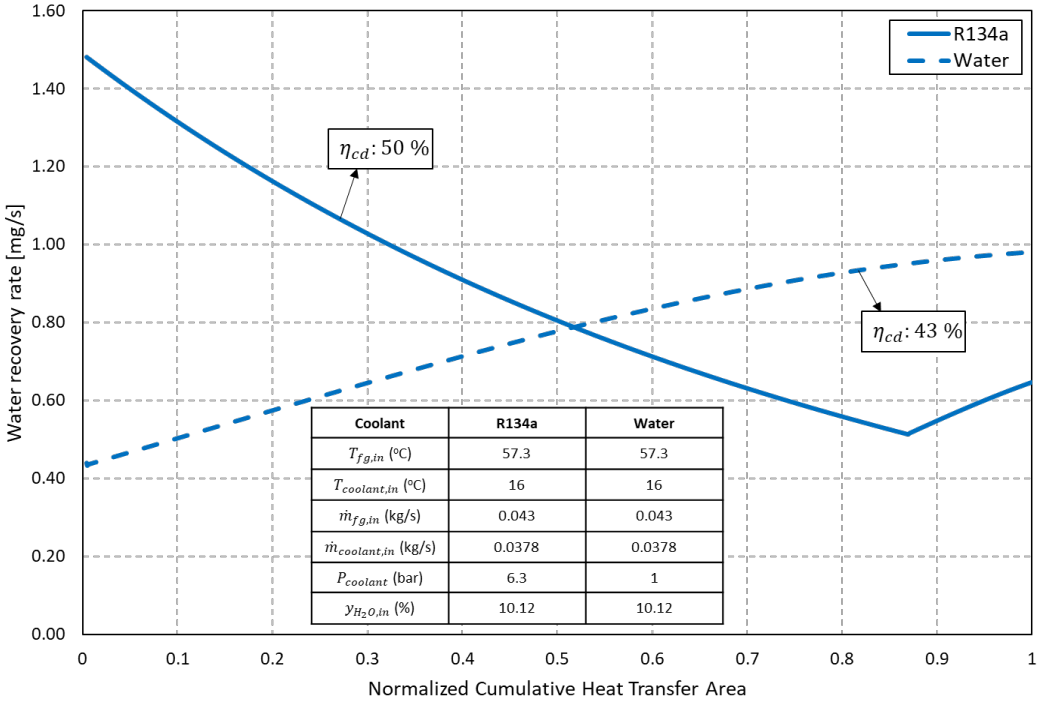

Coolant	R134a	Water
$T_{fg,in}$ (°C)	57.3	57.3
$T_{coolant,in}$ (°C)	16	16
$\dot{m}_{fg,in}$ (kg/s)	0.043	0.043
$\dot{m}_{coolant,in}$ (kg/s)	0.0378	0.0378
$P_{coolant}$ (bar)	6.3	1
$y_{H_2O,in}$ (%)	10.12	10.12

Fig. 11. Calculated water recovery rate along the normalized cumulative heat transfer area for R134a and water coolant

For water coolant case from Fig. 11, calculated local condensation rate of water vapor was increased from 0.43 mg/s to 0.98 mg/s from inlet to exit of flue gas side of heat exchanger. From Fig. 10 (b), it is inferred that molar gradient of water vapor between bulk and interface $(y_{H_2O} - y_i)$ was least at inlet side and maximum at exit side and because of this, the condensation rate was highest at inlet and least at exit. The total condensation rate was calculated by integrating the local condensation rate along the heat exchanger as performed with R134a coolant. The total condensation rate was 1,170 mg/s from total heat transfer area and predicted water recovery efficiency (wt. basis) was 43%. The modelling predicted that R134a was 16% more efficient in water recovery than water coolant. It was established from the modelling that to maximize water recovery efficiency, the molar gradient between water vapor in bulk flue gas and interface should be maximized.

6. Conclusions

An analytical numerical modelling was developed to simulate simultaneous phase transitions in the pilot-scale horizontal cross-flow heat exchanger (LT-E) for water recovery from combustion flue gas using R134a coolant. The governing equations were derived based on mass and energy balance and heat and mass transfer to predict the water condensation rate, and the empirical correlations were used to calculate the two-phase heat transfer during flow-boiling of the refrigerant R134a. The iterative solution technique using one-dimensional forward finite difference method was applied in the modelling to

solve for the governing equations. It was found that the average discrepancy between modelling and test results for R134a coolant for water recovery efficiencies and flue gas exit temperatures were 10% and 3% respectively.

The modelling results on the heat transfer coefficients of R134a showed that heat transfer coefficient for subcooled R134a did not change much, but in the two-phase region, there was increase in two-phase heat transfer coefficient from the inlet to exit of refrigerant due to increase in the void fraction which decreases the density of liquid-vapor mixture and consequently increases the flow velocity of R134a. This increase in flow velocity increases turbulence, which ultimately increases the two phase heat transfer coefficient.

Performance comparison in terms of heat transfer rate and water recovery efficiency was also carried out between the two coolants. It was found that heat exchanger with R134a coolant achieved a higher heat transfer rate and higher water recovery efficiency since isothermal interference temperature during flow-boiling acted as controlling factor to set higher molar gradient between water vapor in bulk flue gas and interface. The modelling results also showed that heat transfer rate and water recovery efficiency (wt.) were 50% and 16% higher in R134a than in water coolant case respectively.

Acknowledgments

This research and paper were prepared with the thankful support of the Korea Institute of Machinery and Materials (KIMM) under the project: Numerical Simulation of Heat and Mass Transfer in Condensing Heat Exchangers for Water and Energy Recovery in Power Plants.

References

[1] C. Dieter, M. Maupin, R. Caldwell, M. Harris, T. Ivahnenko, J. Lovelace, N. Barber and K. Linsey, *Estimated use of water in the United States in 2015*.

[2] Y. Yan and T. Lin, "Evaporation Heat Transfer and Pressure Drop of Refrigerant R-134a in a Plate Heat Exchanger", *Journal of Heat Transfer*, vol. 121, no. 1, pp. 118-127, 1999. Available: 10.1115/1.2825924.

[3] S. Kandlikar and P. Balasubramanian, "An Extension of the Flow Boiling Correlation to Transition, Laminar, and Deep Laminar Flows in Minichannels and Microchannels", *Heat Transfer Engineering*, vol. 25, no. 3, pp. 86-93, 2004. Available: 10.1080/01457630490280425.

[4] S. Kandlikar, "A General Correlation for Saturated Two-Phase Flow Boiling Heat Transfer Inside Horizontal and Vertical Tubes", *Journal of Heat Transfer*, vol. 112, no. 1, pp. 219-228, 1990. Available: 10.1115/1.2910348.

[5] S. Kandlikar, "A Model for Correlating Flow Boiling Heat Transfer in Augmented Tubes and Compact Evaporators", *Journal of Heat Transfer*, vol. 113, no. 4, pp. 966-972, 1991. Available: 10.1115/1.2911229.

[6] A. Greco and G. Vanoli, "Flow-boiling of R22, R134a, R507, R404A and R410A inside a smooth horizontal tube", *International Journal of Refrigeration*, vol. 28, no. 6, pp. 872-880, 2005. Available: 10.1016/j.ijrefrig.2005.01.008.

[7] S. Saitoh, H. Daiguji and E. Hihara, "Correlation for boiling heat transfer of R-134a in horizontal tubes including effect of tube diameter", *International Journal of Heat and Mass Transfer*, vol. 50, no. 25-26, pp. 5215-5225, 2007. Available: 10.1016/j.ijheatmasstransfer.2007.06.019.

[8] K. Choi, A. Pamitran, C. Oh and J. Oh, "Boiling heat transfer of R-22, R-134a, and CO2 in horizontal smooth minichannels", *International Journal of Refrigeration*, vol. 30, no. 8, pp. 1336-1346, 2007. Available: 10.1016/j.ijrefrig.2007.04.007.

[9] C. Tibiriçá and G. Ribatski, "Flow boiling heat transfer of R134a and R245fa in a 2.3mm tube", *International Journal of Heat and Mass Transfer*, vol. 53, no. 11-12, pp. 2459-2468, 2010. Available: 10.1016/j.ijheatmasstransfer.2010.01.038.

[10] K. Jeong, M. Kessen, H. Bilirgen and E. Levy, "Analytical modelling of water condensation in condensing heat exchanger", *International Journal of Heat and Mass Transfer*, vol. 53, no. 11-12, pp. 2361-2368, 2010. Available: 10.1016/j.ijheatmasstransfer.2010.02.004.

[11] J. Copetti, M. Macagnan, F. Zinani and N. Kunsler, "Flow boiling heat transfer and pressure drop of R-134a in a mini tube: an experimental investigation", *Experimental Thermal and Fluid Science*, vol. 35, no. 4, pp. 636-644, 2011. Available: 10.1016/j.expthermflusci.2010.12.013.

[12] K. Jeong, S. Sircar and H. Caram, "Modelling of heat recovery from a steam-gas mixture in a high-temperature sorption process", *AIChE Journal*, vol. 58, no. 1, pp. 312-321, 2011. Available: 10.1002/aic.12564.
[13] S. Kim and I. Mudawar, "Universal approach to predicting saturated flow boiling heat transfer in mini/micro-channels -Part I. Dryout incipience quality", *International Journal of Heat and Mass Transfer*, vol.64, pp. 1226-1238, 2013. Available: 10.1016/j.ijheatmasstransfer.2013.04.016.
[14] X. Fang, "A new correlation of flow boiling heat transfer coefficients based on R134a data", *International Journal of Heat and Mass Transfer*, vol. 66, pp. 279-283, 2013. Available: 10.1016/j.ijheatmasstransfer.2013.07.015.
[15] S. Kim and I. Mudawar, "Review of databases and predictive methods for heat transfer in condensing and boiling mini/micro-channel flows", *International Journal of Heat and Mass Transfer*, vol. 77, pp. 627-652, 2014. Available: 10.1016/j.ijheatmasstransfer.2014.05.036.
[16] D. Sempértegui-Tapia and G. Ribatski, "Flow boiling heat transfer of R134a and low GWP refrigerants in a horizontal micro-scale channel", *International Journal of Heat and Mass Transfer*, vol. 108, pp. 2417-2432, 2017. Available: 10.1016/j.ijheatmasstransfer.2017.01.036.
[17] F. Kanizawa, C. Tibiriçá, G. Ribatski, "Heat transfer during convective flow boiling inside micro-scale channels", International Journal of Mass Transfer, vol. 93, pp. 566-583, 2016.
[18] E. Gorgy and S. Eckels, "Convective boiling of R-134a on enhanced-tube bundles", *International Journal of Refrigeration*, vol. 68, pp. 145-160, 2016. Available: 10.1016/j.ijrefrig.2016.04.010.
[19] Y. Min, A. Negash, S. Shamsi, D. Shin, G. Cho, "Experimental study of labscale organic rankine cycle system for heat and water recovery from flue gas in thermal power plant", *Proceedings of PRES 19, 2019.*
[20] S. Shamsi, A. Negash, G. Cho and Y. Kim, "Waste Heat and Water Recovery System Optimization for Flue Gas in Thermal Power Plants", *Sustainability*, vol. 11, no. 7, p. 1881, 2019. Available: 10.3390/su11071881.
[21] A. Colburn and O. Hougen, "Design of Cooler Condensers for Mixtures of Vapors with Noncondensing Gases", *Industrial & Engineering Chemistry*, vol. 26, no. 11, pp. 1178-1182, 1934. Available: 10.1021/ie50299a011.
[22] G. Thomson, "The Antoine Equation for Vapor-pressure Data.", *Chemical Reviews*, vol. 38, no. 1, pp. 1-39, 1946. Available: 10.1021/cr60119a001.
[23] A. P. Colburn, "Trans. Am. Inst. Chem. Eng.", vol. 29, pp. 174, 1933.
[24] M. Osakabe, "Thermal-hydraulic behavior and prediction of heat exchanger for latent heat recovery of exhaust flue gas", *Proceeding of the ASME Heat Transfer Division*, vol. 2, 1999.
[25] K. Stephen, "Heat Transfer in Condensation and Boiling", Springer-Verlag, New York, 1992.
[26] A. Zhukauskas, "Heat transfer from tubes in cross flow", *Advances Heat Transfer*, vol. 8, Academic Press, 1972.
[27] F.P. Incopera, D.P. Dewitt, T.L. Bergman, A.S. Lavine, "Fundamentals of Heat and Mass Transfer", sixth ed., Wiley,2007.
[28] S. Aryal, "Unsteady modelling on fly ash deposition in full-scale gas-to-gas heaters for ultrasupercritical pulverized coal-fired power plant applications", Master, Arkansas State University, 2018.
[29] S. Aryal, S. Tamang, K. Jeong, J. Lee, S. Lee and H. Seo, "Ash deposition modelling in low temperature heat exchanger for pulverized coal-fired powerplant applications", in *Clearwater Clean Energy Conference*, Florida, 2018.
[30] "Thermophysical Properties of Fluid Systems", *Webbook.nist.gov*, 2020.